3 Biotech (2017) 7:100
DOI 10.1007/s13205-017-0744-3

ORIGINAL ARTICLE

MERS-CoV papain-like protease (PL^{pro}): expression, purification, and spectroscopic/thermodynamic characterization

Ajamaluddin Malik[1] · **Mohammad A. Alsenaidy**[2]

Received: 25 August 2016 / Accepted: 6 February 2017 / Published online: 30 May 2017

Abstract Within a decade, MERS-CoV emerged with nearly four times higher case fatality rate than an earlier outbreak of SARS-CoV and spread out in 27 countries in short span of time. As an emerging virus, combating it requires an in-depth understanding of its molecular machinery. Therefore, conformational characterization studies of coronavirus proteins are necessary to advance our knowledge of the matter for the development of antiviral therapies. In this study, MERS-CoV papain-like protease (PL^{pro}) was recombinantly expressed and purified. Thermal folding pathway and thermodynamic properties were characterized using dynamic multimode spectroscopy (DMS) and thermal shift assay. DMS study showed that the PL^{pro} undergoes a single thermal transition and follows a pathway of two-state folding with T_m and van't Hoff enthalpy values of 54.4 ± 0.1 °C and 317.1 ± 3.9 kJ/mol, respectively. An orthogonal technique based on intrinsic tryptophan fluorescence also showed that MERS-CoV PL^{pro} undergoes a single thermal transition and unfolds via a pathway of two-state folding with a T_m value of 51.4 °C. Our findings provide significant understandings of the thermodynamic and structural properties of MERS-CoV PL^{pro}.

Keywords Differential scanning fluorometry · Dynamic multimode spectroscopy · MERS · Papain-like protease · Thermal shift assay

Abbreviations

Amp	Ampicillin
DTT	Dithiothreitol
EDTA	Ethylenediaminetetraacetic acid
FPLC	Fast protein liquid chromatography
IPTG	Isopropyl β-D-1-thiogalactopyranoside
L	Liter
LB	Luria–Bertani
MPL^{pro}	MERS papain-like protease
Ni-NTA	Nickel-nitrilotriacetic acid
OD_{600}	Optical density at 600 nm
PMSF	Phenylmethylsulfonyl fluoride
rpm	Rotation per minute

Introduction

Frequent fatal coronavirus outbreaks in humans and animals have caused serious concerns in the healthcare sector, scientific community, and animal husbandry. First human outbreak of severe acute respiratory syndrome coronavirus (SARS-CoV) in 2002 caused life-threatening atypical pneumonia in more than 8000 people in 26 countries with a case fatality rate (CFR) of 10% (Pillaiyar et al. 2015; Al-Tawfiq et al. 2014; WHO 2016b). Another lethal coronavirus outbreak emerged in the Arab peninsula countries in 2012 which was caused by what is now known as the Middle East respiratory syndrome coronavirus (MERS-CoV). From September 2012 to December 2016, 1864

✉ Ajamaluddin Malik
amalik@ksu.edu.sa

[1] Department of Biochemistry, Protein Research Chair, College of Science, King Saud University, PO Box 2455, Riyadh 11451, Saudi Arabia

[2] Vaccines and Biologics Research Unit, Department of Pharmaceutics, College of Pharmacy, King Saud University, PO Box 2457, Riyadh 11451, Saudi Arabia

laboratory-confirmed MERS-CoV cases of infection in 27 countries with 659 mortalities (nearly four times higher CFR than SARS-CoV) have been reported (Al-Tawfiq et al. 2016; WHO 2016a). Coronavirus survivors after acute infections suffer from many health issues and require long-term medical assistance (Han et al. 2003; Ong et al. 2005; Chan et al. 2003; Leow et al. 2005; Siu 2016; Cha et al. 2016). In addition to SARS-CoV and MERS-CoV, at least four other pathological coronaviruses (HCoV-OC43, HCoV-229E, HCoV-HKU1, and HCoV-NL63) are continuously circulating in humans causing relatively mild respiratory conditions that may in some instances escalate to severe pathological illnesses (Mackay et al. 2012; Carbajo-Lozoya et al. 2012; Simon et al. 2007). Coronaviruses have also caused deadly diseases in animals, leading to huge economic losses in the animal husbandry sector (Vlasova et al. 2014; Lee and Lee 2014; Sun et al. 2016). Moreover, high mutation and recombination rates in coronaviruses allow them to cross species barriers and adapt to new hosts more easily (Denison et al. 2011; Lau and Chan 2015).

Viral proteases are essential for pathogenesis and virulence. Like all coronaviruses, MERS-CoV contains two cysteine proteases (main protease and papain-like protease) which processes viral nonstructural polypeptides (Kilianski et al. 2013; Hilgenfeld 2014). MERS-CoV main protease (M^{pro}, also called the 3C-like protease, $3CL^{pro}$) cleaves at eleven sites, while MERS-CoV papain-like protease (PL^{pro}) cuts at three sites on the nonstructural polypeptides and releases mature nonstructural proteins (Hilgenfeld 2014). Thus, MERS-CoV proteases make up a suitable target for antiviral therapies.

MERS-CoV open-reading frame 1 (ORF1) encodes two large polyproteins (pp1a and pp1b). MERS-CoV PL^{pro} domain is encoded on the pp1a proteins (residue 1484–1800) (Yang et al. 2014; Hilgenfeld 2014; Kilianski et al. 2013). Like other coronaviruses, MERS-CoV PL^{pro} contains a catalytic triad and exhibits similar proteolytic, deubiquitination, and ISG15-linked ISGylation properties (Lin et al. 2014; Chen et al. 2007; Clementz et al. 2010; Yang et al. 2014; Zheng et al. 2008).

In this study, we expressed and purified MERS-CoV PL^{pro}. Thermal stability was studied by thermal shift assay using intrinsic fluorescence and Dynamic Multimode Spectroscopy (DMS). MERS-CoV PL^{pro} was found to unfold via a single thermal transition and follows a pathway of two-state folding. This study will not only help in the understanding of the folding and stability of MERS-CoV PL^{pro} but also could help shed some light on other deubiquitinating enzymes with the similar folding scaffold.

Materials and methods

Chemicals and instruments

The ORF of MERS-CoV PL^{pro} (1484–1800 polyprotein residues, GenBank accession number NC_019843.2) was cloned into pET28a plasmid under T7 promoter as published before (Lin et al. 2014). The codon was optimized (GenScript, USA) and cloned between NcoI and XhoI sites which was in frame of C-terminal His tag present on the vector. *E. coli* BL21 (DE3) pLysS was used for the expression of recombinant protein. Low-molecular weight protein markers, prepacked Ni-NTA, and Superdex 75 columns were from Amersham Biosciences (United Kingdom). Chicken egg lysozyme was from USB Corporation, USA. Benzonase, ANS, and kanamycin from Sigma. IPTG was purchased from Bio Basic, Canada. All other chemicals used in this study were of reagent grade. Cary 60 spectrometer and Cary Eclipse spectrofluorometer were from Agilent technologies, USA. AKTA purification system was from Amersham Biosciences (United Kingdom) and SDS-PAGE assembly from Bio-Rad (USA). Thermomixer and benchtop cooling centrifuge were from Eppendorf, Germany. Innova 44R Shaking incubator was from New Brunswick, Germany. Chirascan-Plus spectropolarimeter was from Applied photophysics, United Kingdom.

Expression and purification of MERS-CoV PL^{pro} in *E. coli* BL21 (DE3) pLysS

E. coli BL21 (DE3) pLysS harboring pET28a-MPL^{pro} was used for expression of MERS-CoV PL^{pro}. Protein expression and soluble protein extraction were performed as described in Lin et al. (2014). Purification of MERS-CoV PL^{pro} was performed with minor modification of an earlier published protocol (Lin et al. 2014). Briefly, 1 mM DTT was used throughout unless described. Cleared crude lysate was passed through a 1-mL Ni-NTA column pre-equilibrated with 20 mM Tris, pH 8.5, 500 mM NaCl, 10 mM imidazole, and 1 mM DTT and washed with 20 CV equilibration buffer. Bound protein was eluted with a linear gradient of 0–50% Buffer B (equilibration buffer containing 500 mM Imidazole) at 1 mL/min flow rate on AKTA purification system. The purity of eluted fractions was analyzed on SDS-PAGE.

The prepacked Superdex 75 equilibrated with 20 mM Tris, pH 8.5, 100 mM NaCl, and 1 mM DTT was calibrated with proteins of known molecular weight. Subsequently, Ni-NTA-purified MERS-CoV PL^{pro} was further purified using Superdex 75 column. The purity of eluted

fractions was analyzed on SDS-PAGE. Highly pure fractions were pooled, aliquoted, and stored at −80 °C.

Protein quantification

Before analysis, the frozen aliquots were thawed and centrifuged at 13,000 rpm for 15 min at 4 °C. Protein concentration was determined spectrophotometrically at 280 nm using a molar extinction coefficient of 42,400 M^{-1} cm^{-1}.

Fluorescence spectroscopy

Tryptophan fluorescence spectra (50 µg/mL) of MERS-CoV PL^{pro} were recorded using a Cary Eclipse Fluorescence Spectrophotometer in a 10-mm-path length cuvette. To measure tryptophan fluorescence, MERS-CoV PL^{pro} sample was excited at 295 nm and emission spectra were collected between 305 and 400 nm (5 nm excitation and 5 nm emission bandwidth). Temperature melting studies of MERS-CoV PL^{pro} were performed at 10 °C increments as well as a linear increase of 1 °C/min. MERS-CoV PL^{pro} incubated at different temperatures from 20 to 90 °C in Peltier-controlled Cary eclipse fluorometer. The temperature of the protein samples was monitored using an internal temperature probe. When the desired temperature was reached, the sample was allowed to equilibrate for 2 min before tryptophan fluorescence spectra were measured. The maximum fluorescence intensity (I_{max}) and maximum fluorescence wavelength (λ_{max}) were plotted with respect to temperature. In a similar experiment, MERS-CoV PL^{pro} was gradually heated from 20 to 80 °C at a rate of 1 °C/min during which tryptophan fluorescence was measured by exciting at 295 nm and collecting at 330 and 350 nm to obtain the temperature melting curve.

Dynamic multimode spectroscopy

To study the secondary structure of MERS-CoV PL^{pro} in terms of conformational and thermal stability, dynamic multimode spectroscopy was applied. The measurement was performed using Chirascan-Plus spectrophotometer, calibrated with (1S)-(+)-10-camphorsulfonic acid. In this study, 0.2 mg/mL of MERS-CoV PL^{pro} was gradually heated from 20 to 94 °C at 1 °C/mL rate. Internal thermal probe was inserted in the 0.1-cm-path length cuvette to precisely monitor the actual temperature of the samples. Far-UV CD spectra from 200 to 250 nm were recorded at each temperature. Thermal transition data were processed using manufacturer's Global 3 software.

MERS-CoV PL^{pro} activity

The steady-state kinetics of MERS-CoV PL^{pro} was measured as described in Lin et al. (2014), with slight modification. Briefly, 50 µM fluorogenic peptidyl substrate, Dabcyl–FRLKGGAPIKGV–Edans (GenScript), was mixed with different concentrations of MERS-CoV PL^{pro} (6.8–0.1 µM, in twofold serial dilution) using 50 mM phosphate at pH 6.5 as a buffer at room temperature. The fluorescence signal was measured for 30 min at 60-s intervals in a Hidex Chameleon plate reader using 340 nm (excitation) and 535 nm (emission filter) with 20% gain.

Results and discussion

Expression and purification of recombinant MERS-CoV PL^{pro}

In this study, MERS-CoV PL^{pro} was overexpressed in *E. coli* BL21 (DE3) pLysS. MERS-CoV PL^{pro} was purified in two-step chromatography as described in Lin et al. (2014). Ni-NTA elute contained minor impurities (data not shown). When Ni-NTA elute passed through gel filtration column, one major symmetrical sharp peak was obtained (Fig. 1a). SDS-PAGE analysis of the pooled fractions showed the yield of highly pure MERS-CoV PL^{pro} (Fig. 1b). We obtained nearly 10 mg of MERS-CoV PL^{pro} from a 1-L shake flask culture. In an earlier study, the yield of soluble MERS-CoV PL^{pro} was strain dependent and the best yield (~52 mg purified protein from 1 L shake flask culture) was obtained with *E. coli* BL21 (DE3) STAR strain (Lin et al. 2014). The difference in the yield of MERS-CoV PL^{pro} was due to the different strain's genetic background.

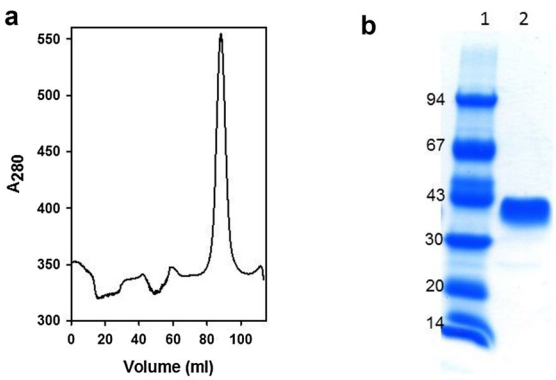

Fig. 1 Purification of His-tagged MERS-CoV PL^{pro}. **a** The Ni-NTA elute was passed through Superdex 75 equilibrated with 20 mM Tris, pH 8.5, 100 mM NaCl, and 1 mM DTT. Protein was eluted in one major symmetrical peak. **b** Fractions were pooled and analyzed on 4–20% gradient SDS-PAGE. *Lane 1* low-molecular weight marker, *lane 2* pooled fractions of MERS-CoV PL^{pro}

Thermal shift assay

Intrinsic fluorescence spectroscopy is a highly sensitive tool, which provides information about the microenvironment of Trp and Tyr residues within proteins. Tyrosine emission maximum is less sensitive to its local environment compared to tryptophan. Indole ring in the tryptophan residues undergoes two isoenergetic transitions which causes polarity sensitivity, while tyrosine undergoes through a single electronic state (Ghisaidoobe and Chung 2014). During the course of protein unfolding, the polarity of fluorophore microenvironment changes, which in turn leads to changes in the maximum fluorescence intensity (I_{max}) as well as maximum fluorescence wavelength (λ_{max}). Therefore, intrinsic tryptophan fluorescence emission is sensitive to the tertiary structure and detects subtle protein conformational changes in solution. It has been frequently used for the characterization of protein's conformational changes under different stress conditions (Kumar et al. 2005; Xiao et al. 2015).

A previous study analyzing the quaternary structure of MERS-CoV PL^{pro} using analytical ultracentrifugation technique has shown that PL^{pro} is found in the monomeric state (Lin et al. 2014). MERS-CoV PL^{pro} contains ten tyrosine and five tryptophan residues (Fig. 2a). MERS-CoV PL^{pro} consists of two domains: N-terminal ubiquitin-like (Ubl) domain and a catalytic core domain. The N-terminal Ubl domain consists of 62 residues and contained one α-helix, one 3_{10}-helix and five β-strands. The substrate-binding region is solvent exposed and comprised of the right-hand scaffold (Lei et al. 2014). Three tryptophan residues (W93, 243 and 303) are buried, while W187 and W190 are surface exposed (Fig. 2b). Figure 3a shows the decrease in intrinsic fluorescence of MERS-CoV PL^{pro} with increasing temperature. At low temperature (20 °C), highest fluorescent intensity (I_{max}) was observed with maximum fluorescence wavelength (λ_{max}) at 343 nm, indicating an overall localization of all five tryptophans in the partially hydrophobic environment. As the temperature increases gradually from 20 to 90 °C, I_{max} decreased with major transitions occurring between 50 and 60 °C (Fig. 3a, b). Initially, λ_{max} increased from 343 to 344 nm when the temperature was increased from 20 to 30 °C. As the temperature was increased further, a blue-shift in λ_{max} with increasing temperature was observed, indicating conformational rearrangements in different temperature regimes. The major blue-shift in λ_{max} was found between 50 and 60 °C (Fig. 3c). The 14-nm blue-shift of tryptophan fluorescence spectrum indicated that the microenvironment of the tryptophan residues is becoming more hydrophobic during thermal denaturation. MERS-CoVPL^{pro} thermal unfolding is different from most other proteins. Commonly, protein unfolding fluorescence spectra are characterized by a long wavelength shift "red-shift." But some proteins,

a

MGTIEVLVTVDGVNFRTVVLNNKNTYRSQLGCVFFNGADISDTIPDEKQNGHSLYLADNLTADETKALKE
LYGPVDPTFLHRFYSLKAAVHKWKMVVCDKVRSLKLSDNNCYLNAVIMTLDLLKDIKFVIPALQHAFMK
HKGGDSTDFIALIMAYGNCTFGAPDDASRLLHTVLAKAELCCSARMVWREWCNVCGIKDVVLQGLKAC
CYVGVQTVEDLRARMTYVCQCGGERHRQIVEHTTPWLLLSGTPNEKLVTTSTAPDFVAFNVFQGIETAVG
HYVHARLKGGLILKFDSGTVSKTSDWKCKVTDVLFPGQKYSSLEHHHHHH

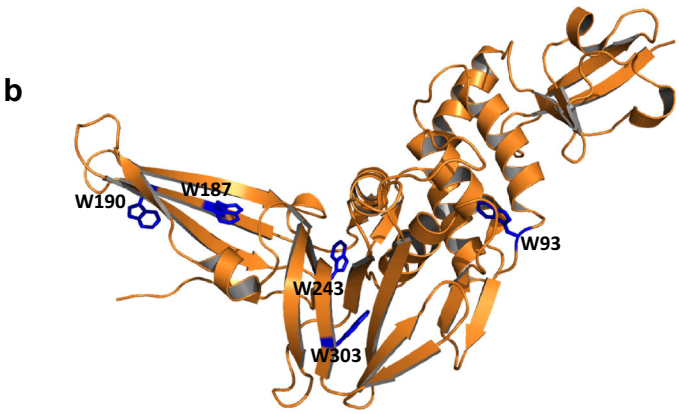

Fig. 2 **a** Sequence of C-terminal His-tagged MERS-CoV PL^{pro} showing ten Tyr and five Trp residues, which are highlighted in *green* and *blue*, respectively. Potential internal protease site is highlighted in *red* and His-tagged residues are *underlined*. **b** Three-dimensional structure of MERS-CoV PL^{pro} (PDB ID: 4R3D) with the side chains of the five Trp residues being *numbered* and colored in *blue*

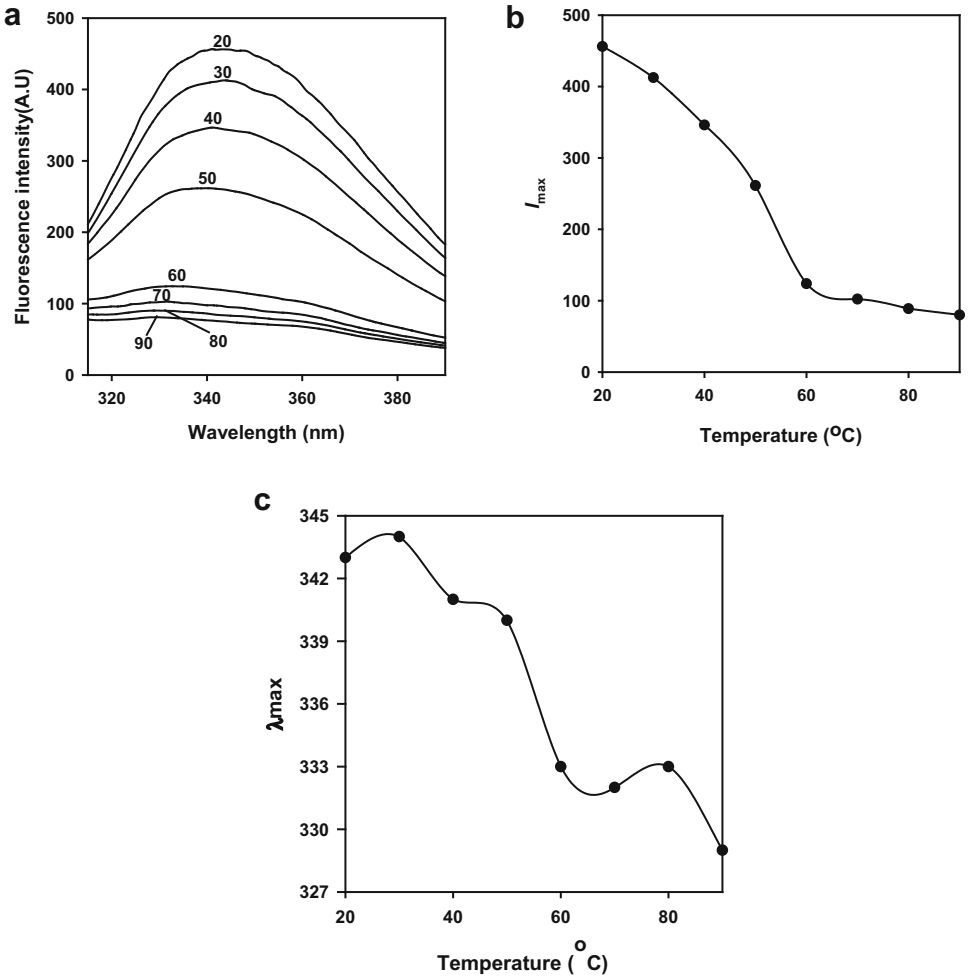

Fig. 3 Thermally induced structural changes in MERS-CoV PL^{pro} as monitored by the intrinsic tryptophan fluorescence spectroscopy. **a** To monitor tryptophan fluorescence at different temperatures, MERS-CoV PL^{pro} was slowly heated and allowed to equilibrate for 2 min at the respective temperatures. The sample was excited at 295 nm and the emission spectra were collected from 305 to 400 nm (5 nm excitation and 5 nm emission bandwidth). **b** Effect of temperature on the tryptophan emission intensity showing the decrease of I_{max} with increasing temperature. Major transition occurred between 50 and 60 °C. **c** Effect of temperature on the tryptophan maximum emission wavelength (λ_{max}). *Blue-shift* was observed during thermal unfolding of MERS-CoV PL^{pro}. Initially, *red-shift* was observed when the temperature was increased from 20 to 30 °C. Further increase in temperature leads to *blue-shift* with major changes occurring between 50 and 60 °C

including MERS-CoV PL^{pro}, exhibit blue-shift upon denaturation (Slutskaya et al. 2015; Duy and Fitter 2006; Pattanaik et al. 2003). Pig pancreatic α-amylase showed red-shifted fluorescence spectra when chemically unfolded and showed blue-shifted spectra during thermal unfolding (Duy and Fitter 2006). Equine lysozyme first exhibits a blue-shift transition at lower temperature and red-shift above 50 °C (Morozova et al. 1991).

To obtain temperature melting curve, MERS-CoVPL^{pro} was gradually heated from 20 to 80 °C at 1 °C/min and the ratio of 330/350 nm tryptophan fluorescence was plotted with respect to temperature (Fig. 4). Data were fitted according to the equation $f = y_0 + a/(1 + \exp(-(x - x_0)/b))$ with an r^2 value of 0.9910. Our results showed that MERS-CoV PL^{pro} was moderately stable and unfolds via a single transition with a T_m value of 51.4 °C.

Since MERS-CoV PL^{pro} is a protease, it may undergo autolysis during thermal shift assay. It contains one potential autolysis site (LKGG) as shown in Fig. 2a. To evaluate the extent of autolysis as well as the extent of irreversible thermal unfolding and aggregation, MERS-CoV PL^{pro} (0.2 mg/mL) was incubated on a thermomixer from 20 to 70 °C with 10 °C intervals. Six samples were gradually heated and equilibrated at the respective temperatures for 3 min. When the desired temperatures were attained, the samples were removed, kept on ice, and centrifuged at 13,000 rpm for 15 min to remove any forming aggregates. Equal volumes of the supernatant were analyzed (Fig. 5). If MERS-CoV PL^{pro} would undergo autolysis during the course of thermal incubation, we would expect to see the appearance of two or more bands of MERS-CoV PL^{pro} fragments on SDS-PAGE gels or at least a decrease in the band intensity of MERS-CoV PL^{pro}. We found that the intensity of MERS-CoV PL^{pro} band was apparently unchanged, indicating that autolysis was not occurring during the thermal shift assays applied in this study. In another scenario, irreversible unfolding aggregates may form during thermal shift assay. If this is the case, then aggregated protein will be pelleted down upon centrifugation and band intensity would have decreased in the supernatant sample. Our result showed that the band intensity of the supernatant samples incubated from 20 to 70 °C was apparently unchanged (Fig. 5), indicating

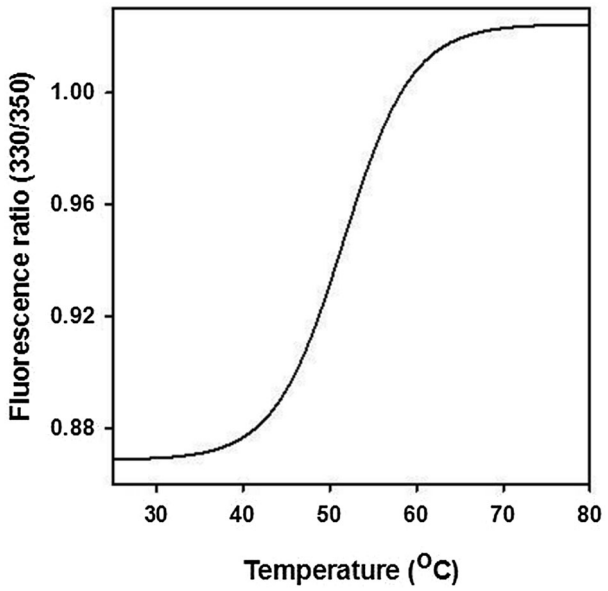

Fig. 4 Thermal shift assay using tryptophan fluorescence. MERS-CoV PL^{pro} was continuously heated from 20 to 80 °C at 1 °C/min and the sample was excited at 295 nm at each temperature and emission spectra at 330 and 350 nm were recorded. The ratio of 330 nm/350 nm was plotted as a function of temperature. The *mid-point* of transition was identified as the thermal melting point (T_m)

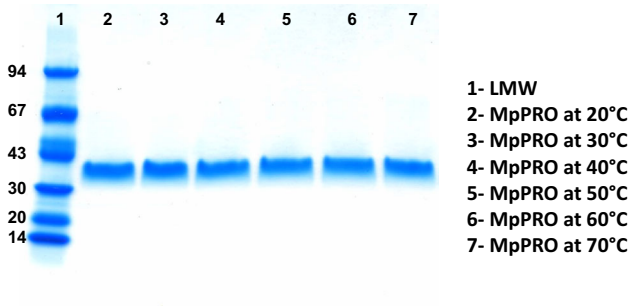

Fig. 5 Autolysis and solubility of MERS-CoV PL^{pro} at different temperatures. MERS-CoV PL^{pro} was incubated at different temperatures. Subsequently, MERS-CoV PL^{pro} was cooled on ice and centrifuged to remove aggregated protein. An equal volume of each sample was analyzed on SDS-PAGE

no or insignificant aggregation occurring during thermal shift assays.

Dynamic multimode spectroscopy (DMS)

Information about thermal stability, unfolding pathway, and secondary structure of MERS-CoV PL^{pro} was obtained using an orthogonal method. We employed DMS, a newly developed information-rich experimental technique, to obtain spectroscopic and thermodynamic data of melting temperature (T_m) and van't Hoff enthalpy (ΔH_{VH}) (John and Weeks 2000; Greenfield 2006; Al-Ahmady et al. 2012). Temperature-induced secondary structural changes in MERS-CoV PL^{pro} in the far-UV region were monitored to study thermodynamic parameters. Moreover, DMS also characterized thermal unfolding pathway and identified the number of folding intermediate species and their relative concentrations during the unfolding process (Malik et al. 2015, 2016). MERS-CoV PL^{pro} was gradually heated from 20 to 94 °C at 1 °C/min increments and far-UV CD spectra were recorded from 200 to 250 nm. Far-UV CD spectra at several wavelengths were plotted as a function of temperature (Fig. 6a). MERS-CoV PL^{pro} underwent a single thermal transition as a function of temperature, suggesting two-state folding. Similar transition was also observed in the thermal shift assay using fluorescence spectroscopy. In an earlier study, secondary structure content was calculated and it was found that β-sheet structure (31%) is dominant in MERS-CoV PL^{pro} (Lin et al. 2014). Similarly, our results showed that MERS-CoV PL^{pro} presented a single negative minimum at ~218 nm suggesting a predominant β-sheet structure as well. When MERS-CoV PL^{pro} was gradually heated, secondary structure was lost and became irregularly disorder structure (Fig. 6b). The relative concentrations of folded and unfolded species as a function of temperature are shown in Fig. 6c. The thermal melting point (T_m) and van't Hoff enthalpy (ΔH_{VH}) of MERS-CoV PL^{pro} calculated using Global 3 analysis software were 54.4 ± 0.1 °C and 317.1 ± 3.9 kJ/mol, respectively. The thermal melting points (T_m) of MERS-CoV PL^{pro} calculated by thermal shift assay and DMS were found to be in close proximity, reflecting tertiary–secondary structure unfolding events, respectively. In a recent study, papain-like protease of Murine Coronavirus also underwent a single thermal transition with a T_m value of ~46 °C (Mielech et al. 2015). A three-dimensional model of the thermal transitions of MERS-CoV PL^{pro} was generated using Global 3 analysis software (Fig. 6d). A single transition is clearly evident at lower wavelengths in the far-UV spectra region.

Conclusions

MERS-CoV PL^{pro} was expressed in soluble state in *E. coli* and purified to homogeneity in two-step chromatography. Two orthogonal techniques were used for studying unfolding pathway that include the utilization of DMS and thermal shift assay. The results showed that MERS-CoV PL^{pro} unfolds via a single thermal transition and follows a two-state unfolding pathway. Thermal shift assay calculated a T_m value of 51.4 °C and DMS method calculated a T_m value of 54.4 ± 0.1 °C, in agreement with sequential unfolding events of tertiary and secondary structures, respectively. Similar folding behavior and thermal melting point were also observed in papain-like protease of Murine

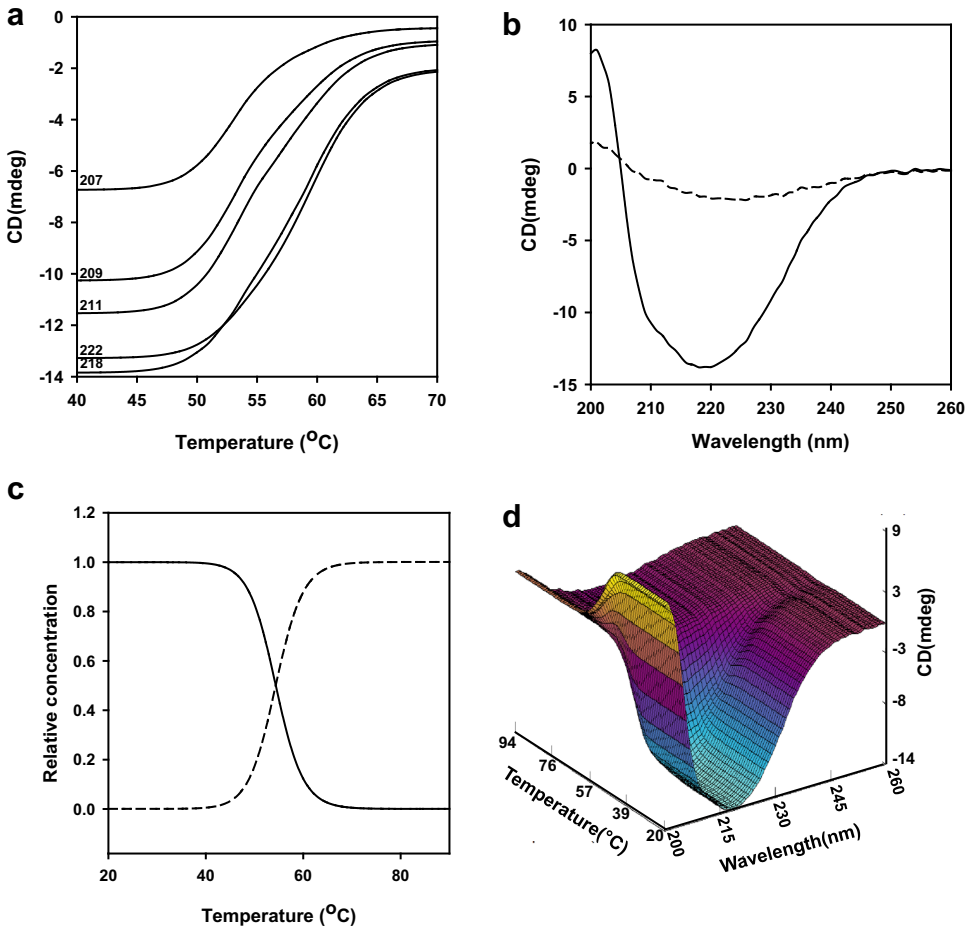

Fig. 6 Dynamic multimode spectroscopy: temperature-induced structural changes in MERS-CoV PL^{pro} plotted as a function of temperature and wavelength. **a** Temperature-induced structural changes in MERS-CoV PL^{pro} at different wavelengths. Far-UV CD spectra were shown in mdeg units at selected wavelengths. Global 3 software was used for calculating thermal transitions. Single thermal transitions were found at the wavelengths between 207 and 222 nm. **b** Calculated far-UV CD spectra of the MERS-CoV PL^{pro} folding species. At 20 °C, MERS-CoV PL^{pro} predominantly adopts β-sheet conformation as shown in *solid line*. The unfolded state of MERS-CoV PL^{pro} is shown in *dashed line* with much of its structure being lost. **c** Calculated concentration profiles of the MERS-CoV PL^{pro} folding species during thermal-induced unfolding process. The figure shows the relative concentrations of thermal-induced disappearance and appearance of the folded species. The relative concentration of MERS-CoV PL^{pro} in folded state is shown in solid line and unfolded species in *dashed line*. **d** Calculated far-UV CD, wavelength, and temperature three-dimensional graph. The 3D model of MERS-CoV PL^{pro} unfolding was calculated with the help of Global 3 software

Coronavirus, indicating similarity in deubiquitinating enzyme scaffold. Next, we have planned to evaluate the effect of different factors such as pH and ionic strength on the folding, conformational stability, and protease activity of MERS-CoV PL^{pro}. Such studies will facilitate in exploring the different stability profiles of the different conformations as well as in evaluating the environmental condition affecting higher-order structural states in an effort to develop antivirals.

Acknowledgements The authors extend their appreciation to the Deanship of Scientific Research at King Saud University for funding this work through the Research Project No R5-16-02-05.

Compliance with ethical standards

Conflict of interest To the best of our knowledge, no conflict of interest, financial or others, exists. All authors are fully aware of this submission.

References

Al-Ahmady ZS, Al-Jamal WT, Bossche JV, Bui TT, Drake AF, Mason AJ, Kostarelos K (2012) Lipid-peptide vesicle nanoscale hybrids for triggered drug release by mild hyperthermia in vitro and in vivo. ACS Nano 6(10):9335–9346. doi:10.1021/nn302148p

Al-Tawfiq JA, Zumla A, Memish ZA (2014) Travel implications of emerging coronaviruses: SARS and MERS-CoV. Travel Med Infect Dis 12(5):422–428. doi:10.1016/j.tmaid.2014.06.007

Al-Tawfiq JA, Omrani AS, Memish ZA (2016) Middle East respiratory syndrome coronavirus: current situation and travel-associated concerns. Front Med 10(2):111–119. doi:10.1007/s11684-016-0446-y

Carbajo-Lozoya J, Muller MA, Kallies S, Thiel V, Drosten C, von Brunn A (2012) Replication of human coronaviruses SARS-CoV, HCoV-NL63 and HCoV-229E is inhibited by the drug FK506. Virus Res 165(1):112–117. doi:10.1016/j.virusres.2012.02.002

Cha RH, Yang SH, Moon KC, Joh JS, Lee JY, Shin HS, Kim DK, Kim YS (2016) A case report of a middle east respiratory syndrome survivor with kidney biopsy results. J Korean Med Sci 31(4):635–640. doi:10.3346/jkms.2016.31.4.635

Chan KS, Zheng JP, Mok YW, Li YM, Liu YN, Chu CM, Ip MS (2003) SARS: prognosis, outcome and sequelae. Respirology 8(Suppl):S36–S40

Chen Z, Wang Y, Ratia K, Mesecar AD, Wilkinson KD, Baker SC (2007) Proteolytic processing and deubiquitinating activity of papain-like proteases of human coronavirus NL63. J Virol 81(11):6007–6018. doi:10.1128/JVI.02747-06

Clementz MA, Chen Z, Banach BS, Wang Y, Sun L, Ratia K, Baez-Santos YM, Wang J, Takayama J, Ghosh AK, Li K, Mesecar AD, Baker SC (2010) Deubiquitinating and interferon antagonism activities of coronavirus papain-like proteases. J Virol 84(9):4619–4629. doi:10.1128/JVI.02406-09

Denison MR, Graham RL, Donaldson EF, Eckerle LD, Baric RS (2011) Coronaviruses: an RNA proofreading machine regulates replication fidelity and diversity. RNA Biol 8(2):270–279

Duy C, Fitter J (2006) How aggregation and conformational scrambling of unfolded states govern fluorescence emission spectra. Biophys J 90(10):3704–3711. doi:10.1529/biophysj.105.078980

Ghisaidoobe AB, Chung SJ (2014) Intrinsic tryptophan fluorescence in the detection and analysis of proteins: a focus on Forster resonance energy transfer techniques. Int J Mol Sci 15(12):22518–22538. doi:10.3390/ijms151222518

Greenfield NJ (2006) Using circular dichroism collected as a function of temperature to determine the thermodynamics of protein unfolding and binding interactions. Nat Protoc 1(6):2527–2535. doi:10.1038/nprot.2006.204

Han Y, Geng H, Feng W, Tang X, Ou A, Lao Y, Xu Y, Lin H, Liu H, Li Y (2003) A follow-up study of 69 discharged SARS patients. J Tradit Chin Med 23(3):214–217

Hilgenfeld R (2014) From SARS to MERS: crystallographic studies on coronaviral proteases enable antiviral drug design. FEBS J 281(18):4085–4096. doi:10.1111/febs.12936

John DM, Weeks KM (2000) van't Hoff enthalpies without baselines. Protein Sci 9(7):1416–1419. doi:10.1110/ps.9.7.1416

Kilianski A, Mielech AM, Deng X, Baker SC (2013) Assessing activity and inhibition of Middle East respiratory syndrome coronavirus papain-like and 3C-like proteases using luciferase-based biosensors. J Virol 87(21):11955–11962. doi:10.1128/JVI.02105-13

Kumar V, Sharma VK, Kalonia DS (2005) Second derivative tryptophan fluorescence spectroscopy as a tool to characterize partially unfolded intermediates of proteins. Int J Pharm 294(1–2):193–199. doi:10.1016/j.ijpharm.2005.01.024

Lau SK, Chan JF (2015) Coronaviruses: emerging and re-emerging pathogens in humans and animals. Virol J 12:209. doi:10.1186/s12985-015-0432-z

Lee S, Lee C (2014) Outbreak-related porcine epidemic diarrhea virus strains similar to US strains, South Korea, 2013. Emerg Infect Dis 20(7):1223–1226. doi:10.3201/eid2007.140294

Lei J, Mesters JR, Drosten C, Anemuller S, Ma Q, Hilgenfeld R (2014) Crystal structure of the papain-like protease of MERS coronavirus reveals unusual, potentially druggable active-site features. Antiviral Res 109:72–82. doi:10.1016/j.antiviral.2014.06.011

Leow MK, Kwek DS, Ng AW, Ong KC, Kaw GJ, Lee LS (2005) Hypocortisolism in survivors of severe acute respiratory syndrome (SARS). Clin Endocrinol (Oxf) 63(2):197–202. doi:10.1111/j.1365-2265.2005.02325.x

Lin MH, Chuang SJ, Chen CC, Cheng SC, Cheng KW, Lin CH, Sun CY, Chou CY (2014) Structural and functional characterization of MERS coronavirus papain-like protease. J Biomed Sci 21:54. doi:10.1186/1423-0127-21-54

Mackay IM, Arden KE, Speicher DJ, O'Neil NT, McErlean PK, Greer RM, Nissen MD, Sloots TP (2012) Co-circulation of four human coronaviruses (HCoVs) in Queensland children with acute respiratory tract illnesses in 2004. Viruses 4(4):637–653. doi:10.3390/v4040637

Malik A, Haroon A, Jagirdar H, Alsenaidy AM, Elrobh M, Khan W, Alanazi MS, Bazzi MD (2015) Spectroscopic and thermodynamic properties of recombinant heat shock protein A6 from *Camelus dromedarius*. Eur Biophys J 44(1–2):17–26. doi:10.1007/s00249-014-0997-2

Malik A, Fouad D, Labrou NE, Al-Senaidy AM, Ismael MA, Saeed HM, Ataya FS (2016) Structural and thermodynamic properties of kappa class glutathione transferase from Camelus dromedarius. Int J Biol Macromol 88:313–319. doi:10.1016/j.ijbiomac.2016.03.065

Mielech AM, Deng X, Chen Y, Kindler E, Wheeler DL, Mesecar AD, Thiel V, Perlman S, Baker SC (2015) Murine coronavirus ubiquitin-like domain is important for papain-like protease stability and viral pathogenesis. J Virol 89(9):4907–4917. doi:10.1128/JVI.00338-15

Morozova L, Haezebrouck P, Van Cauwelaert F (1991) Stability of equine lysozyme. I. Thermal unfolding behaviour. Biophys Chem 41(2):185–191

Ong KC, Ng AW, Lee LS, Kaw G, Kwek SK, Leow MK, Earnest A (2005) 1-year pulmonary function and health status in survivors of severe acute respiratory syndrome. Chest 128(3):1393–1400. doi:10.1378/chest.128.3.1393

Pattanaik P, Ravindra G, Sengupta C, Maithal K, Balaram P, Balaram H (2003) Unusual fluorescence of W168 in *Plasmodium falciparum* triosephosphate isomerase, probed by single-tryptophan mutants. Eur J Biochem 270(4):745–756

Pillaiyar T, Manickam M, Jung S-H (2015) Middle East respiratory syndrome-coronavirus (MERS-CoV): an updated overview and pharmacotherapeutics. Med Chem 5(8):361–372

Simon A, Volz S, Hofling K, Kehl A, Tillman R, Muller A, Kupfer B, Eis-Hubinger AM, Lentze MJ, Bode U, Schildgen O (2007) Acute life threatening event (ALTE) in an infant with human coronavirus HCoV-229E infection. Pediatr Pulmonol 42(4):393–396. doi:10.1002/ppul.20595

Siu JY (2016) Coping with future epidemics: Tai chi practice as an overcoming strategy used by survivors of severe acute respiratory syndrome (SARS) in post-SARS Hong Kong. Health Expect 19(3):762–772. doi:10.1111/hex.12270

Slutskaya E, Artemova N, Kleymenov S, Petrova T, Popov V (2015) Heat-induced conformational changes of TET peptidase from crenarchaeon *Desulfurococcus kamchatkensis*. Eur Biophys J 44(8):667–675. doi:10.1007/s00249-015-1064-3

Sun D, Wang X, Wei S, Chen J, Feng L (2016) Epidemiology and vaccine of porcine epidemic diarrhea virus in China: a mini-review. J Vet Med Sci 78(3):355–363. doi:10.1292/jvms.15-0446

Vlasova AN, Marthaler D, Wang Q, Culhane MR, Rossow KD, Rovira A, Collins J, Saif LJ (2014) Distinct characteristics and

complex evolution of PEDV strains, North America, May 2013–February 2014. Emerg Infect Dis 20(10):1620–1628. doi:10.3201/eid2010.140491

WHO (2016a) Middle East respiratory syndrome coronavirus (MERS-CoV). http://www.who.int/emergencies/mers-cov/en/. Accessed 02 Jan 2017

WHO (2016b) SARS (Severe Acute Respiratory Syndrome). http://www.who.int/ith/diseases/sars/en/. Accessed 16 Jun 2016

Xiao QJ, Li ZG, Yang J, He Q, Xi L, Du LF (2015) Heat-induced unfolding of apo-CP43 studied by fluorescence spectroscopy and CD spectroscopy. Photosynth Res 126(2–3):427–435. doi:10.1007/s11120-015-0166-1

Yang X, Chen X, Bian G, Tu J, Xing Y, Wang Y, Chen Z (2014) Proteolytic processing, deubiquitinase and interferon antagonist activities of Middle East respiratory syndrome coronavirus papain-like protease. J Gen Virol 95(Pt 3):614–626. doi:10.1099/vir.0.059014-0

Zheng D, Chen G, Guo B, Cheng G, Tang H (2008) PLP2, a potent deubiquitinase from murine hepatitis virus, strongly inhibits cellular type I interferon production. Cell Res 18(11):1105–1113. doi:10.1038/cr.2008.294